Bound on thermoelectric power in a magnetic field within linear response

Kay Brandner and Udo Seifert
II. Institut für Theoretische Physik, Universität Stuttgart, 70550 Stuttgart, Germany
(Received 30 September 2014; revised manuscript received 4 December 2014; published 12 January 2015)

For thermoelectric power generation in a multiterminal geometry, strong numerical evidence for a universal bound as a function of the magnetic-field induced asymmetry of the nondiagonal Onsager coefficients is presented. This bound implies, *inter alia*, that the power vanishes at least linearly when the maximal efficiency is approached. In particular, this result rules out that Carnot efficiency can be reached at finite power, which an analysis based on the second law only would, in principle, allow.

DOI: 10.1103/PhysRevE.91.012121 PACS number(s): 05.70.Ln, 72.15.Jf, 84.60.Bk

I. INTRODUCTION

Thermoelectric generators use a heat current between two reservoirs of temperatures T_h and $T_c < T_h$ connected via a device to drive a particle current against a gradient in chemical potential, thus delivering useful power. As a fundamental consequence of the second law of thermodynamics, the efficiency η of such a heat engine is bounded by the Carnot value $\eta_C \equiv 1 - T_c/T_h$. This bound can indeed be reached if the device acts as a perfect energy filter [1]; however, only at the price of vanishing power [2,3].

The relationship between thermoelectric power and efficiency beyond this limiting case has been widely studied during the past few years [4–9], see also Refs. [10,11] for recent reviews. A particular landmark was achieved by Whitney [12,13], who calculated the transmission function that leads to optimal efficiency at given power and thereby identified upper bounds on the output power of quantum coherent devices. In all cases, however, finite power is only possible at an efficiency strictly smaller than η_C.

This antivalence resembles the power-efficiency dilemma, which has been studied by Allahverdyan *et al.* on the basis of a quite general model for a reciprocating quantum heat engine [14]. Their results confirm the general expectation that, under realistic conditions, a conventional cyclic heat engine can approach Carnot efficiency only in the quasistatic limit, within which its power output necessarily goes to zero.

In strong contrast, Benenti *et al.* have recently pointed out that a magnetic field, which breaks the symmetry between the off-diagonal Onsager coefficients, might enhance the efficiency of a thermoelectric heat engine substantially such that η_C seems to be achievable even at finite power [15]. This exciting suggestion follows from a straightforward analysis of the linear response regime using only the second law. However, so far, neither a specific model for a thermoelectric generator delivering finite power at Carnot efficiency, nor a fundamental principle forbidding the existence of such a super device has been discovered.

A promising platform for the investigation of both of these aspects is provided by the multiterminal setup sketched in Fig. 1. By operating this model as a thermoelectric heat engine, we previously derived bounds on its efficiency η that are stronger than the ones obtained by Benenti *et al.* [16,17]. These bounds, which follow from current conservation, depend only on the number n of terminals and, for any finite n, constrain η to be strictly smaller than η_C whenever the off-diagonal Onsager coefficients are not identical, thus preventing finite power at Carnot efficiency.

In this paper, we move an essential step forward by investigating whether not only efficiency but also power can be bounded. Since power P carries a physical dimension, such an endeavor can be expected to be harder and, *a priori*, less universal, than searching for a bound on the dimensionless efficiency. Bounding power is arguably more relevant since a high efficiency is useless from a practical point of view if it comes with minuscule power. Here we provide strong numerical evidence that P is indeed subject to a new bound. This bound implies that the power output of the device vanishes whenever its efficiency approaches the upper limit corresponding to the respective number of terminals. Finally, by extrapolating our findings to arbitrary n, we derive a conjecture for a universal bound on P, which rules out the option of finite power at Carnot efficiency even in the limit $n \to \infty$.

The paper is organized as follows. In Sec. II, we give give a brief review of the essentials of the multiterminal model and the bounds on its efficiency as a thermoelectric heat engine, which were derived in our previous work [16,17]. Section III contains our main results. We outline the numerical procedure used to substantiate our new constraint on the Onsager coefficients and show how this constraint can be used to bound the power of the multiterminal thermoelectric generator. Finally, we conclude in Sec. IV.

II. MULTITERMINAL MODEL

A. Setup

We consider the model sketched in Fig. 1. On the primary level, n electronic reservoirs of respective temperature T_i and chemical potential μ_i ($i = h,1,\ldots,n-2,c$) are connected via perfect, one-dimensional leads to a central scattering region penetrated by the magnetic field $\mathbf{B}$. The particle and heat currents flowing from the reservoir i to the scattering region are denoted by J^i_ρ and J^i_q, the corresponding affinities by

$$\mathcal{F}^i_\rho \equiv (\mu_i - \mu)/T \quad \text{and} \quad \mathcal{F}^i_q \equiv (T_i - T)/T^2, \qquad (1)$$

respectively, where the reference values $\mu = \mu_c$ and $T = T_c$ have been chosen. In the linear response regime, to which we will stick throughout the paper, the phenomenological equations describing the coupled heat and particle transport

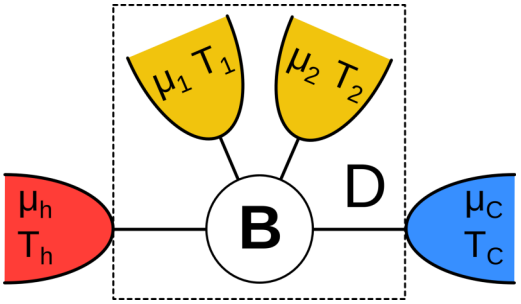

FIG. 1. (Color online) Sketch of a thermoelectric generator. Both heat and particle current run from the hot reservoir on the left to the cold reservoir on the right, thereby traversing the device D, which is represented by the dashed box. Within the multiterminal setup, the device consists of a central scattering region subject to a magnetic field $\mathbf{B}$ and $n-2$ probe terminals. The figure corresponds to $n=4$.

in this system read

$$\mathbf{J}^i = \sum_{j=\mathrm{h},\ldots,n-2} \mathbb{L}_{ij}\boldsymbol{\mathcal{F}}^j \tag{2}$$

with $\mathbf{J}^i \equiv (J^i_\rho, J^i_q)^t$, $\boldsymbol{\mathcal{F}}^i \equiv (\mathcal{F}^i_\rho, \mathcal{F}^i_q)^t$, and $\mathbb{L}_{ij} \in \mathbb{R}^{2\times 2}$ for $i,j = h,1,\ldots,n-2$. Since, at this stage, we assume uncorrelated particles, which move coherently through the leads and the scattering region, the matrix blocks $\mathbb{L}_{ij}$ can be calculated explicitly using the multiterminal Landauer formula [18,19]

$$\mathbb{L}_{ij} = \int_0^\infty dE\; f(E) \begin{pmatrix} 1 & E-\mu \\ E-\mu & (E-\mu)^2 \end{pmatrix} [\delta_{ij} - \mathcal{T}_{ij}(E)] \tag{3}$$

with $f(E) \equiv \cosh^{-2}((E-\mu)/(2k_BT))/(4k_Bh)$, where h denotes Planck's constant and k_B Boltzmann's constant. The energy- and magnetic-field-dependent transmission coefficients $\mathcal{T}_{ij}(E)$ encode the properties of the scattering region and cover the effects of particle-particle interactions on the mean-field level [20]. Due to current conservation and time-reversal symmetry, these dimensionless quantities must fulfill the sum rules [18,19],

$$\sum_{i=h,\ldots,c} \mathcal{T}_{ij}(E) = \sum_{j=h,\ldots,c} \mathcal{T}_{ij}(E) = 1 \tag{4}$$

and the symmetry relation

$$\mathcal{T}_{ij}(E,\mathbf{B}) = \mathcal{T}_{ji}(E,-\mathbf{B}), \tag{5}$$

respectively. Throughout the paper, we notationally suppress the dependence of any quantity on $\mathbf{B}$ if there is no need to indicate it explicitly. For vanishing magnetic field, relation (5) implies that the primary Onsager matrix showing up in Eq. (2) must be symmetric. For a fixed $\mathbf{B} \neq 0$, however, (5) does not lead to any further constraint.

The full multiterminal setup described above becomes a model for a thermoelectric heat engine by imposing the boundary conditions $J^i_\rho = J^i_q = 0$ for $i = 1,\ldots,n-2$. Using these constraints to eliminate the corresponding affinities $\mathcal{F}^i_\rho, \mathcal{F}^i_q$, we obtain the reduced set of phenomenological equations

$$\begin{pmatrix} J^h_\rho \\ J^h_q \end{pmatrix} = \begin{pmatrix} L_{\rho\rho} & L_{\rho q} \\ L_{q\rho} & L_{qq} \end{pmatrix} \begin{pmatrix} \mathcal{F}^h_\rho \\ \mathcal{F}^h_q \end{pmatrix}, \tag{6}$$

where the $L_{\alpha\beta}$ with $\alpha,\beta = \rho,q$ denote effective Onsager coefficients, which are given by

$$\begin{aligned} &\begin{pmatrix} L_{\rho\rho} & L_{\rho q} \\ L_{q\rho} & L_{qq} \end{pmatrix} \\ &\quad = \mathbb{L}_{hh} - (\mathbb{L}_{h1},\ldots,\mathbb{L}_{hn-2}) \\ &\qquad \times \begin{pmatrix} \mathbb{L}_{11} & \cdots & \mathbb{L}_{1n-2} \\ \vdots & \ddots & \vdots \\ \mathbb{L}_{n-21} & \cdots & \mathbb{L}_{n-2\,n-2} \end{pmatrix}^{-1} \begin{pmatrix} \mathbb{L}_{1h} \\ \vdots \\ \mathbb{L}_{n-2h} \end{pmatrix}, \end{aligned} \tag{7}$$

with $\mathbb{L}_{ij}$ the blocks of primary Onsager coefficients defined in Eq. (3).

The physical intuition behind this procedure is that only the hot and the cold terminal are considered as real, while the remaining ones act as probes, which do not exchange any net quantities with the physical reservoirs. Originally proposed by Büttiker [21], such probe terminals have meanwhile become a well-established method to phenomenologically model inelastic scattering events like electron-phonon interactions, see, for example, Refs. [16,17,22–24]. Such processes would be hard to take into account on a microscopic level, but are, *inter alia*, crucial to obtain a nonsymmetric Onsager matrix [25,26].

B. Bounds on efficiency

The thermodynamic efficiency of a thermoelectric generator in the linear response regime generally reads

$$\eta \equiv \frac{P}{J^h_q} = -\eta_C \frac{L_{\rho\rho}\gamma^2 + L_{\rho q}\gamma}{L_{q\rho}\gamma + L_{qq}}, \tag{8}$$

where

$$P = (\mu - \mu_h)J^h_\rho = -T\left(\mathcal{F}^h_q\right)^2 (L_{\rho\rho}\gamma^2 + L_{\rho q}\gamma) \tag{9}$$

is the supplied power,

$$\gamma \equiv \mathcal{F}^h_\rho / \mathcal{F}^h_q \tag{10}$$

denotes the ratio of the affinities, and $\eta_C \equiv (T_h - T)/T = T\mathcal{F}^h_q$ is the linear response expression of the Carnot efficiency. Maximizing η with respect to γ yields the maximum efficiency

$$\eta_{\max}(x,y) \equiv \eta_C x \frac{\sqrt{y+1}-1}{\sqrt{y+1}+1}. \tag{11}$$

Here we introduced the dimensionless parameters

$$x \equiv \frac{L_{\rho q}}{L_{q\rho}} \quad \text{and} \quad y \equiv \frac{L_{\rho q}L_{q\rho}}{L_{\rho\rho}L_{qq} - L_{\rho q}L_{q\rho}}, \tag{12}$$

which, due to the second law, have to obey the inequalities [15]

$$h(x) \leqslant y \leqslant 0 \quad \text{for} \quad x < 0, \quad 0 \leqslant y \leqslant h(x) \quad \text{for} \quad x > 0 \tag{13}$$

with $h(x) \equiv 4x/(x-1)^2$. For $\mathbf{B} = 0$, x assumes the symmetric value 1 as a consequence of time-reversal symmetry and y reduces to the conventional figure of merit ZT [15,27].

In our previous work on the n-terminal setup [17], we showed that current conservation implies that (13) can be strengthened by replacing $h(x)$ with

$$h_n(x) \equiv \frac{4x\cos^2(\pi/n)}{(x-1)^2}. \tag{14}$$

The resulting constraint leads to the bound

$$\eta_{\max}(x) \equiv \eta_C x \frac{\sqrt{h_n(x)+1}-1}{\sqrt{h_n(x)+1}+1} \tag{15}$$

on the efficiency as a function of the asymmetry parameter x, which, for any finite number of terminals, is stronger than the one required by the bare second law. However, no predictions on a putative maximal power can be drawn from the analysis presented so far.

III. BOUNDS ON POWER

The fundamental bound on power discussed in this paper follows from the constraint

$$\bar{L}_{qq} \equiv L_{qq}/N_{qq} \leqslant 1 - y/h_n(x) \tag{16}$$

on the Onsager coefficient L_{qq}, where

$$N_{qq} \equiv \frac{k_B^2 T^3 q}{4h} \tag{17}$$

is a dimensional factor with q defined in Eq. (20). We find this constraint, which constitutes our first main result, by randomly generating transmission matrices obeying the sum rules (4) and exploiting the matrix structure (3).

A. Numerical procedure and results

Our aim for this subsection is to numerically confirm the constraint (16). Since it is convenient to work with dimensionless quantities, we first change the integration variable in Eq. (3) as $\varepsilon \equiv (E-\mu)/(k_B T)$ and, second, define the rescaled matrix blocks

$$\begin{aligned}\bar{\mathbb{L}}_{ij} &\equiv \int_{-\nu}^{\infty} d\varepsilon\ \bar{f}(\varepsilon) \begin{pmatrix} 1/p & \varepsilon/\sqrt{pq} \\ \varepsilon/\sqrt{pq} & \varepsilon^2/q \end{pmatrix} [\delta_{ij} - \bar{\mathcal{T}}_{ij}(\varepsilon)] \\ &\equiv \mathbb{D}\mathbb{L}_{ij}\mathbb{D},\end{aligned} \tag{18}$$

where

$$\mathbb{D} \equiv \sqrt{\frac{4h}{T}} \begin{bmatrix} 1/\sqrt{p} & 0 \\ 0 & 1/(k_B T\sqrt{q}) \end{bmatrix}, \tag{19}$$

$\bar{f}(\varepsilon) \equiv \cosh^{-2}(\varepsilon/2)$ and $\bar{\mathcal{T}}_{ij}(\varepsilon) \equiv \mathcal{T}_{ij}(\varepsilon k_B T + \mu)$. The scaling parameters p and q are defined by

$$\begin{pmatrix} p \\ q \end{pmatrix} \equiv \int_{-\nu}^{\infty} d\varepsilon\ \bar{f}(\varepsilon) \begin{pmatrix} 1 \\ \varepsilon^2 \end{pmatrix} \xrightarrow{\nu\to\infty} \begin{pmatrix} 4 \\ 4\pi^2/3 \end{pmatrix}, \tag{20}$$

where $\nu \equiv \mu/k_B T$.[1]

[1]The explicit evaluation of the integral showing up in Eq. (20) for finite ν yields

$$p = 2[1+\tanh(\nu/2)]$$

$$q = 2\nu\{\nu - 4\ln(1+e^{\nu}) + \nu\tanh(\nu/2)\} - 8\mathrm{Li}_2(-e^{\nu}),$$

where Li_2 denotes the dilogarithm.

Next, to obtain a tractable parametrization of the matrix blocks (18), we make use of the fact that the matrix $\bar{\mathbb{T}}(\varepsilon)$ with elements $(\bar{\mathbb{T}}(\varepsilon))_{ij} \equiv \bar{\mathcal{T}}_{ij}(\varepsilon)$ is bistochastic, i.e., for any fixed ε, its elements fulfill the same sum rules (4) as the $\mathcal{T}_{ij}(E)$. Consequently, by virtue of the Birkhoff-von Neumann theorem, there is a set of N permutation matrices $\mathbb{P}^k$ and positive numbers $\lambda_k(\varepsilon)$ such that

$$\bar{\mathbb{T}}(\varepsilon) = \sum_{k=1}^{N} \lambda_k(\varepsilon)\mathbb{P}^k \quad \text{and} \quad \sum_{k=1}^{N} \lambda_k(\varepsilon) = 1. \tag{21}$$

Inserting this decomposition into (18) and formally carrying out the integral yields

$$\bar{\mathbb{L}}_{ij} = \sum_{k=1}^{N} \left(\delta_{ij} - P_{ij}^k\right) \cdot \mathbb{M}_k, \tag{22}$$

where the $P_{ij}^k \equiv (\mathbb{P}^k)_{ij}$ are the matrix elements of the respective permutation matrix and

$$\mathbb{M}_k \equiv \int_{-\nu}^{\infty} d\varepsilon\ \bar{f}(\varepsilon)\lambda_k(\varepsilon) \begin{pmatrix} 1/p & \varepsilon/\sqrt{pq} \\ \varepsilon/\sqrt{pq} & \varepsilon^2/q \end{pmatrix} \tag{23}$$

is a positive semidefinite, symmetric matrix of dimension 2. Due to these properties of the $\mathbb{M}_k$, there exist some numbers $\sigma_k, a_k \in (0,\infty)$, $w_k \in [-1,1]$, such that

$$\mathbb{M}_k = \sigma_k \begin{pmatrix} 1 & w_k a_k \\ w_k a_k & a_k^2 \end{pmatrix}. \tag{24}$$

Combining this expression for $\mathbb{M}_k$ with the decomposition (22) gives a parameterization of the dimensionless matrix blocks $\bar{\mathbb{L}}_{ij}$ in terms of N permutation matrices $\mathbb{P}^k$ of dimension n and $3N$ real parameters σ_k, a_k, w_k. The latter are constrained by the two important sum rules

$$\sum_{k=1}^{N} \sigma_k = \sum_{k=1}^{N} \sigma_k a_k^2 = 1, \tag{25}$$

which follow directly by comparing (24) with (23) and using the sum rule (21) for the $\lambda_k(\varepsilon)$. We note that, in principle, there is a third sum rule,

$$\begin{aligned}\sqrt{pq}\sum_{k=1}^{N} \sigma_k w_k a_k &= \int_{-\nu}^{\infty} d\varepsilon\ \bar{f}(\varepsilon)\varepsilon \\ &= \ln(16) + 4\ln(\cosh(\nu/2)) - 2\nu\tanh(\nu/2).\end{aligned} \tag{26}$$

However, for simplicity, this constraint will not be exploited within our analysis.

We now proceed as follows. First, we chose a fixed set of N distinct, n-dimensional permutation matrices $A_P \equiv \{\mathbb{P}^k\}_{k=1}^N$ and randomly pick a large number of parameter sets $A_M \equiv \{\sigma_k, a_k, w_k\}_{k=1}^N$ such that for any of these sets the sum rules (25) are fulfilled. Second, for any of the sets A_M, we evaluate the matrix blocks $\bar{\mathbb{L}}_{ij}$ according to (24) and (22) and subsequently calculate the rescaled effective Onsager matrix $\bar{\mathbb{L}}$ using (7) with the $\mathbb{L}_{ij}$ replaced by $\bar{\mathbb{L}}_{ij}$. Third, for any individual of the thus obtained matrices $\bar{\mathbb{L}}$, we determine the values of the parameters x and y by inserting the elements of $\bar{\mathbb{L}}$ into the definitions given in Eq. (12). This step is justified, since it is readily seen that the effective Onsager matrix $\mathbb{L}$ is connected to

its rescaled counterpart via the transformation $\mathbb{L} = \mathbb{D}^{-1}\bar{\mathbb{L}}\mathbb{D}^{-1}$ and therefore the scaling factors contained in $\mathbb{D}$ cancel if the elements of $\mathbb{L}$ are plugged into (12). Finally, we plot the rescaled Onsager coefficient $\bar{L}_{qq}$, i.e., the lower right entry of the matrix $\bar{\mathbb{L}}$, against the ratio $y/h_n(x)$. This choice of variables is quite reasonable, since, as we will show in the next subsection, the maximum power of the multiterminal thermoelectric generator is proportional to $L_{qq} = N_{qq}\bar{L}_{qq}$ and we are especially interested in the behavior of this quantity as y approaches its bound $h_n(x)$.

We begin with the minimal cases $n = 3$ and $n = 4$. Figure 2 shows the results of the procedure outlined above for two representative sets A_P of respectively three permutation matrices and all w_k randomly chosen from an increasingly large interval. We observe that for any of these models the inequality (16) is respected and, for some of them, even saturated. Our numerical data further suggests that this bound is independent of the choice and number N of distinct permutation matrices $\mathbb{P}^k$ in the set A_P, where N must be larger than two and at least one of the $\mathbb{P}^k$ has to be nonsymmetric to obtain a nonsymmetric effective Onsager matrix. However, if N is increased, it becomes more and more improbable to find models, for which $\bar{L}_{qq}$ attains the bound (16) or comes even close to it. Likewise, we find that as the interval Δ, from which the w_k are drawn, is enlarged, the sharp boundary visible in the plots shown in Fig. 2 deteriorates rapidly. Therefore, we are convinced that the data presented in the first row of Fig. 2 cover a representative subset of the extreme points in the given parameter space with respect to the inequality (16).

For $n > 4$, in Fig. 3, we show representative data, which have been obtained for $N = 3$ permutation matrices $\mathbb{P}_k$ and $|w_k| = 1$. The bound (16) holds for any of the randomly chosen models. However, in contrast to the cases $n = 3$ and $n = 4$, we were not able to achieve saturation. Even by increasing the number N beyond 3, this finding persists. Sampling the absolute values of the w_k from a finite interval Δ, like for 3 and 4 terminals, leads to a decay of the sharp boundary lines appearing in Fig. 3. It therefore remains an open question at this stage whether for $n > 4$ there are models that saturate the bound (16).

B. Maximum power

We will now demonstrate in two steps that the new bound (16) significantly restricts the power supplied by a multiterminal thermoelectric generator. First, we maximize (9) with respect to γ, thus obtaining the maximum power

$$P_{\max}(x,y) = T\left(\mathcal{F}_q^h\right)^2 L_{qq}\frac{xy}{4(1+y)}. \tag{27}$$

Second, replacing L_{qq} by its upper bound (16), as indicated from now on by a hat, and optimizing the resulting expression with respect to y gives the upper bound[2]

$$\hat{P}_{\max}(x) \equiv \hat{P}_{\max}(x,y^*(x)) \equiv P_0 x\frac{\sqrt{h_n(x)+1}-1}{\sqrt{h_n(x)+1}+1}, \tag{28}$$

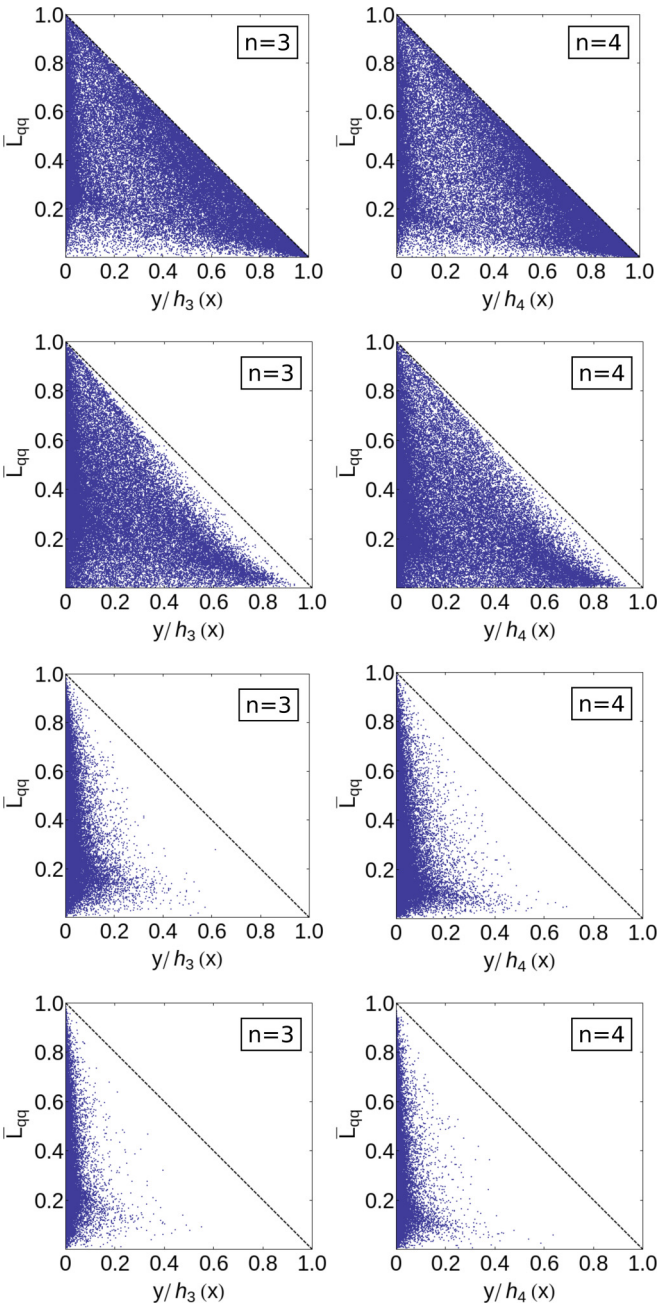

FIG. 2. (Color online) Scatter plots of the rescaled Onsager coefficient $\bar{L}_{qq}$ as a function of the ratio $y/h_n(x)$ for respectively 50 000 randomly chosen n-terminal models. The dashed line is given by $\bar{L}_{qq} = 1 - y/h_n(x)$. To generate these data, we used the set of permutations {(1)(2,3),(1,3)(2),(1,3,2)} for $n = 3$ (left column) and the set {(1)(2)(3,4),(1,4)(2,3),(1,4,2,3)} for $n = 4$ (right column). While for all plots the sign of the w_k is chosen randomly, $|w_k|$ is sampled from an increasingly large interval $\Delta \subseteq [0,1]$. Specifically, we have from the first to the fourth line $\Delta = [1,1]$, $\Delta = [0.99,1]$, $\Delta = [0.5,1]$, $\Delta = [0,1]$.

where

$$P_0 \equiv T\left(\mathcal{F}_q^h\right)^2 N_{qq}/4 \tag{29}$$

sets the scale and $y^*(x) \equiv \sqrt{h_n(x)+1} - 1$. The bound (28), which is our second main result, is plotted in Fig. 4. In

[2]Remarkably, our new bound (28) shows the same functional dependence on x as the bound (15) on the maximum efficiency.

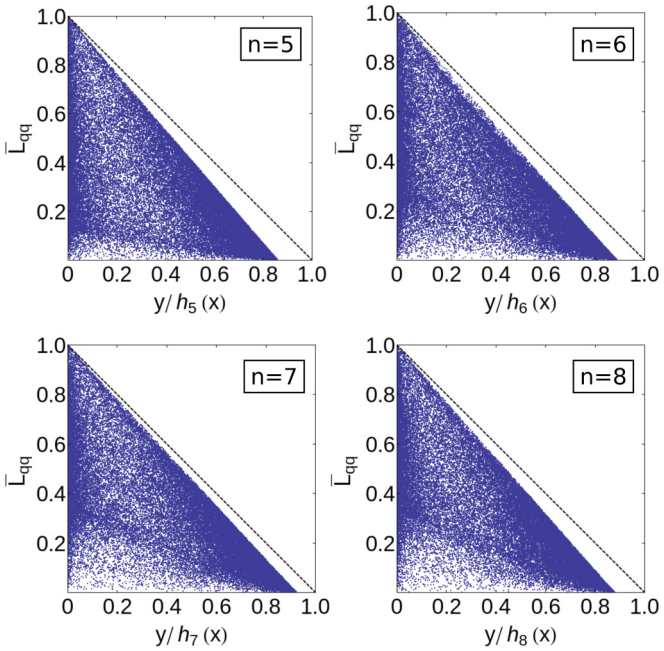

FIG. 3. (Color online) Scatter plots of the rescaled Onsager coefficient $\bar{L}_{qq}$ as a function of the ratio $y/h_n(x)$ for respectively 50 000 randomly chosen n-terminal models. For all plots, the sign of the w_k is chosen by random and their absolute value has been set to $|w_k| = 1$. The sets of permutations used to generate the shown data are {(1,3)(2)(4,5),(1)(2,4)(3,5),(1,4,3,2,5)} for $n = 5$, {(1)(2)(3,6)(4,5),(1,6,4,2,5,3),(1,6,4)(2,3,5)} for $n = 6$, {(1,3)(2,4)(5)(6,7),(1,5,7)(2,6)(3,4),(1,7,4,5,2,6,3)} for $n = 7$, and {(1,6)(2,8)(3,4,7,5),(1,7,6,3,2,8,5)(4),(1,5,4) (2,3)(6,8)(7)} for $n = 8$.

the limit $x \to \pm\infty$, $\hat{P}_{\max}$ asymptotically reaches the value $P_0 \cos^2(\pi/n)$ and, irrespectively of n, $\hat{P}_{\max}(x)$ attains the global maximum P_0 for $x = 1$. Moreover, Fig. 4 reveals that the bound (28) becomes successively weaker as the number of terminals is increased. In particular for $n \to \infty$, $\hat{P}_{\max}(x)$ is equal to P_0 whenever $|x| \geqslant 1$.

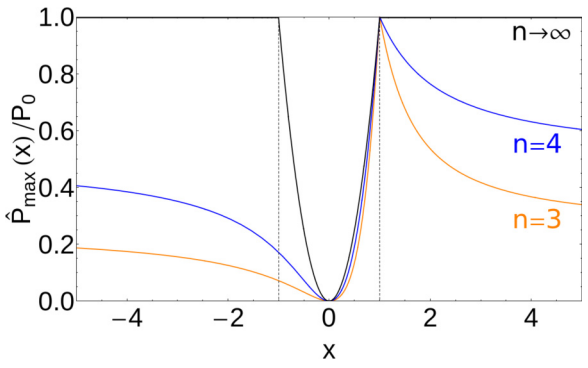

FIG. 4. (Color online) Bound (28) on the rescaled maximum power output $\hat{P}_{\max}(x)/P_0$ of the multiterminal thermoelectric generator as a function of the asymmetry parameter x for $n = 3$, $n = 4$, and $n \to \infty$.

C. Bounding power by efficiency

It is instructive to express the results obtained so far also as a function of the efficiency defined in Eq. (8). To this end, we fix the normalized efficiency $\bar{\eta} \equiv \eta/\eta_C$ by putting

$$\gamma = \frac{-(\bar{\eta}L_{q\rho} + L_{\rho q}) \pm \sqrt{(\bar{\eta}L_{q\rho} + L_{\rho q})^2 - 4\bar{\eta}L_{\rho\rho}L_{qq}}}{2L_{\rho\rho}}. \tag{30}$$

Inserting this γ into the general expression (9) for the power, replacing L_{qq} with its upper bound (16), and expressing the result in terms of the parameters x and y yields a bound $\hat{P}_{\pm}(\eta,x,y)$, whose rather involved expression is given in the appendix. By maximizing this function with respect to y, we obtain the upper bound $\hat{P}_{\max}(x,\eta)$ on power for given efficiency η, asymmetry parameter x, and number of terminals n, which is plotted in Fig. 5. We find that $\hat{P}_{\max}(\eta,x)$ vanishes linearly whenever η approaches its previously identified upper bound (15). Moreover, in the limit $n \to \infty$, for which the bound $\hat{P}_{\max}(\eta,x)$ becomes the weakest, we end up with the remarkably simple expression

$$\hat{P}_{\max}(\eta,x) = 4P_0 \begin{cases} \bar{\eta}(1-\bar{\eta}) & \text{for} \quad |x| \geqslant 1 \\ \bar{\eta} - \bar{\eta}^2/x^2 & \text{for} \quad |x| < 1 \end{cases}, \tag{31}$$

which becomes independent of x for $|x| \geqslant 1$. In particular, (31) shows that the power must vanish at least as $(4P_0/\eta_C)(\eta_C - \eta)$ whenever η approaches the Carnot value. We therefore can conclude that the new constraint (16) rules out the option of finite power at Carnot efficiency for any system that can be described by a multiterminal model with an arbitrary number of probe terminals. This insight is our third main result.

D. Power at maximum efficiency

After having determined the maximum power of the n-terminal model as a heat engine for given efficiency η, as another quantity of particular interest, we will now investigate power at maximum efficiency. To this end, we recall that the maximum efficiency (11) of a thermoelectric generator in the linear response regime is found by optimizing the general expression (8) with respect to γ under the condition $P \geqslant 0$. Inserting the thus-determined γ into (9) gives the power at maximum efficiency,

$$P^*(x,y) = T\left(\mathcal{F}_q^{\mathrm{h}}\right)^2 L_{qq} \frac{x}{\sqrt{1+y}} \frac{\sqrt{1+y}-1}{\sqrt{1+y}+1}. \tag{32}$$

By estimating L_{qq} in terms of its upper bound (16) and eliminating y in favor of $\eta_{\max}$ using (11), we obtain the bound

$$\hat{P}^*(x,\eta_{\max}) = 4P_0\bar{\eta}_{\max}\left[\frac{h_n(x)(x-\bar{\eta}_{\max})^2 - 4x\bar{\eta}_{\max}}{h_n(x)\left(x^2 - \bar{\eta}_{\max}^2\right)}\right] \tag{33}$$

on the power output at maximum efficiency, where $\bar{\eta}_{\max} \equiv \eta_{\max}/\eta_C$.

Figure 6 shows plots of the function $\hat{P}^*(x,\eta_{\max})$ for $n = 3$, $n = 4$, and $n \to \infty$. For any finite n, this function shows a nontrivial global maximum. Specifically, we find the maximum $\simeq 0.726P_0$ at $(x,\bar{\eta}_{\max}) \simeq (1.132,0.422)$ for $n = 3$ and the maximum $\simeq 0.779P_0$ at $(x,\bar{\eta}_{\max}) \simeq (1.373,0.432)$ for $n = 4$. For $n \to \infty$, the global maximum converges to P_0. However, this value can be reached only asymptotically

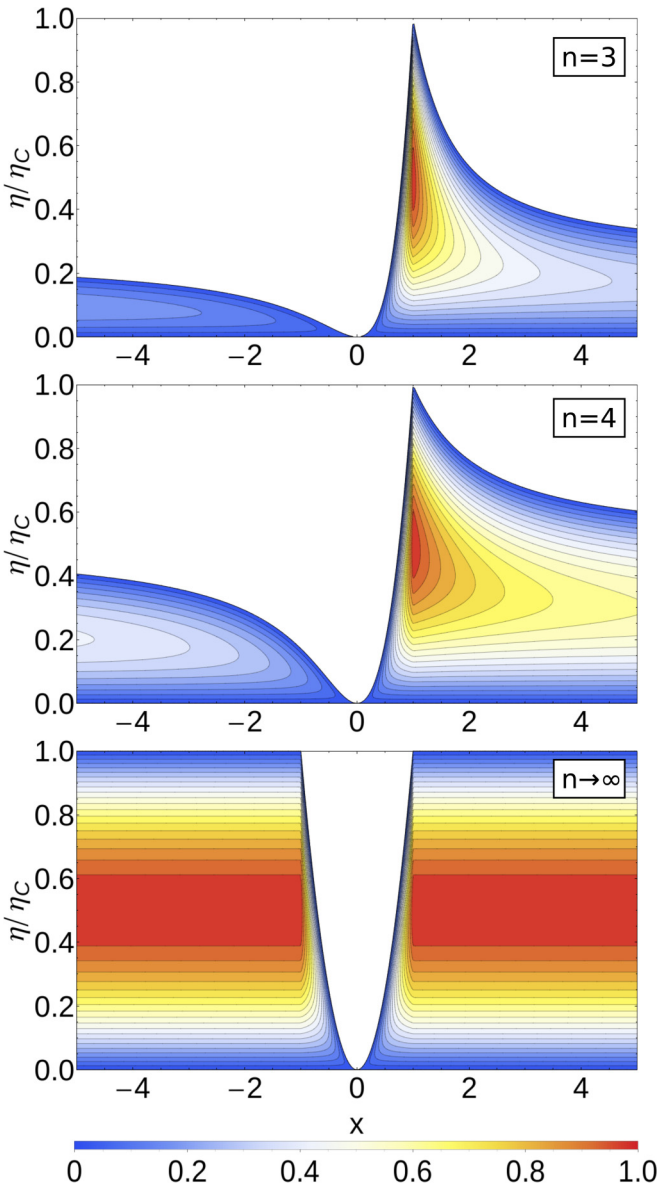

FIG. 5. (Color online) Bounds on the power $\hat{P}_{\max}(\eta,x)$ of the n-terminal model as a thermoelectric heat engine in units of P_0 and as functions of the asymmetry parameter x and the efficiency η for $n = 3,4$ and $n \to \infty$. The white regions in the plots are forbidden by the bound (15).

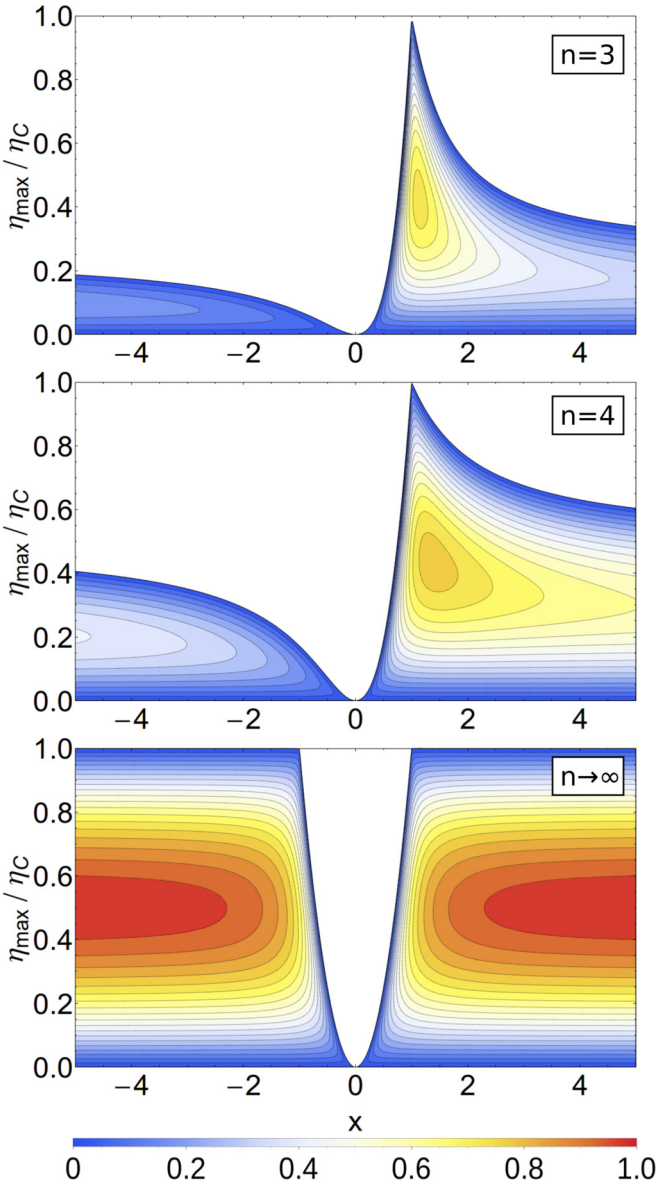

FIG. 6. (Color online) Plots of the bound (33) on the power at maximum efficiency of a n-terminal thermoelectric generator in units of P_0 and as functions of the asymmetry parameter x and the maximum efficiency $\eta_{\max}$ for $n = 3$, $n = 4$, and $n \to \infty$.

for $\bar{\eta}_{\max} = 1/2$ and $x \to \pm\infty$. Moreover, we find that, independent of the number of terminals n and the value of the asymmetry parameter x, the power at maximum efficiency vanishes like $(4P_0/\eta_C)(\eta_{\max}(x) - \eta_{\max})$ when $\eta_{\max}$ saturates its upper bound (15).

IV. CONCLUDING PERSPECTIVES

Strong numerical evidence let us to identify the new constraint (16) on the Onsager coefficients describing the coupled heat and particle transport in the presence of a magnetic field within the paradigmatic multiterminal model for a thermoelectric generator. We emphasize that our numerical scheme uses only the sum rules (4) and the structure (3) of the matrix blocks of which the primary Onsager matrix in Eq. (2) is composed. In particular, the only property of the function $f(E)$ showing up in Eq. (3) that enters our calculations is $f(E) \geqslant 0$ for any $E \geqslant 0$. Therefore, although here provided for a quantum system, with a properly adjusted normalization constant N_{qq} the constraint (16) and all of its consequences likewise hold for classical models like the railway switch model [28] and the recently proposed classical Nernst engine [29] for which $f(E)$ becomes proportional to the Boltzmann factor.

In the second part, we used the constraint (16) to derive an upper bound on the power output (28) as a function of the asymmetry parameter x that quantifies the extent to which an externally applied magnetic field locally breaks the time-reversal symmetry of the dynamics inside the scattering

region. In the symmetric case $x = 1$ and for $\mu = 0$ our bound assumes the value $\hat{P}_{\max}(x = 1) = (1/24)\pi^2 k_B^2 \Delta T^2/h$ with $\Delta T \equiv T_h - T$, which is about a factor of 1.3 larger than the bound $P_{\text{gen}}^{\text{qb2}} \simeq 0.0321 N \pi^2 k_B^2 \Delta T^2/h$ for a single conduction channel, i.e., $N = 1$, which was derived by Whitney [12,13] for a quantum coherent conductor in the nonlinear regime for vanishing magnetic field. The deviation can be explained by the fact that our numerical algorithm does not exploit all features of the primary Onsager matrix that result from the structure of formula (3). Therefore, the constraint (16) and the bounds it implies should not be necessarily regarded as tight, even though they seem to be quite good as the comparison with Withney's result for a special parameter value shows.

Finally, we analyzed the consequences of (16) for the relationship between power and efficiency of the multiterminal model as a thermoelectric generator. We found that, for any n, the maximum power for given η must vanish linearly when η approaches its upper bound (15). Moreover, it turned out that, for $n \to \infty$, the constraint (16) implies the bound (31), which is independent of the asymmetry parameter x for $|x| \geqslant 1$ and comprises the bound $\hat{P}_{\max}(\eta,x)$ for any finite n. Therefore, the assumption that any type of inelastic scattering or interaction between electrons can be mimicked by a sufficient number of probe terminals attached to the scattering region tempts us to speculate that, up to the normalization constant P_0, the bound (31) is universal beyond the multiterminal model. At the current stage, however, an algebraic proof of (16) within this setup as well as a putative derivation of (31) from first principles without reference to a specific model class constitute challenging topics for future research.

APPENDIX: CALCULATION OF THE MAXIMUM POWER FOR GIVEN EFFICIENCY

The function $\hat{P}_{\pm}(\eta,x,y)$ obtained by the procedure described in Sec. III C after Eq. (30) reads

$$\hat{P}_{\pm}(\eta,x,y) = -4P_0\left[1 - \frac{y}{h_n(x)}\right]\frac{\bar{\eta}y}{1+y}\left[\frac{x+\bar{\eta}}{2x} - \frac{1+y}{y} \mp \frac{1}{x}\sqrt{\frac{(x+\bar{\eta})^2}{4} - \frac{x(1+y)\bar{\eta}}{y}}\right], \tag{A1}$$

where $\bar{\eta} \equiv \eta/\eta_C$ denotes the normalized efficiency and y is subject to the constraint

$$\frac{4x\bar{\eta}}{(x-\bar{\eta})^2} \leqslant y \leqslant h_n(x) \quad \text{for} \quad x > 0,$$
$$h_n(x) \leqslant y \leqslant \frac{4x\bar{\eta}}{(x-\bar{\eta})^2} \quad \text{for} \quad x < 0. \tag{A2}$$

Since it is readily seen that $P_+(\eta,x,y) \geqslant P_-(\eta,x,y)$ and we are interested in an upper bound on power, from here onward we will only consider $P_+(\eta,x,y)$. With respect to y, this function assumes its maximum at

$$y^*(x,\eta) \equiv \bar{\eta}\frac{2x + (2x-\bar{\eta})h_n(x) + \sqrt{1+h_n(x)}[2x + (x-\bar{\eta})h_n(x)]}{x^2 - 2x\bar{\eta} + (\bar{\eta}-x)^2 h_n(x)}. \tag{A3}$$

Consequently, the function $\hat{P}_{\max}(\eta,x)$ discussed in Sec. III C and plotted in Fig. 5 is given by

$$\hat{P}_{\max}(\eta,x) \equiv P_+(\eta,x,y^*(x,\eta)). \tag{A4}$$

We note that, in the limit $n \to \infty$, (A3) reduces to

$$\frac{4x\bar{\eta}}{(x-1)(1+x-2\bar{\eta})} \quad \text{for} \quad |x| \geqslant 1, \qquad \frac{4\bar{\eta}}{x - x^3 - 2\bar{\eta} + 2x\bar{\eta}} \quad \text{for} \quad |x| < 1 \tag{A5}$$

and (A4) assumes the simple form (31).

[1] G. D. Mahan and J. O. Sofo, Proc. Natl. Acad. Sci. USA **93**, 7436 (1996).
[2] T. E. Humphrey, R. Newbury, R. P. Taylor, and H. Linke, Phys. Rev. Lett. **89**, 116801 (2002).
[3] T. E. Humphrey and H. Linke, Phys. Rev. Lett. **94**, 096601 (2005).
[4] M. Esposito, K. Lindenberg, and C. Van den Broeck, Eur. Phys. Lett. **85**, 60010 (2009).
[5] M. Leijnse, M. R. Wegewijs, and K. Flensberg, Phys. Rev. B **82**, 045412 (2010).
[6] N. Nakpathomkun, H. Q. Xu, and H. Linke, Phys. Rev. B **82**, 235428 (2010).
[7] R. Sánchez, B. Sothmann, A. N. Jordan, and M. Büttiker, New. J. Phys. **15**, 125001 (2013).
[8] D. M. Kennes, D. Schuricht, and V. Meden, Eur. Phys. Lett. **102**, 57003 (2013).
[9] F. Mazza, R. Bosisio, G. Benenti, V. Giovannetti, R. Fazio, and F. Taddei, New. J. Phys. **16**, 085001 (2014).
[10] G. Benenti, G. Casati, T. Prosen, and K. Saito, arXiv:1311.4430v1 (2013).
[11] B. Sothmann, R. Sánchez, and A. N. Jordan, Nanotechnology **26**, 032001 (2015).
[12] R. S. Whitney, Phys. Rev. Lett. **112**, 130601 (2014).
[13] R. S. Whitney, arXiv:1408.3348 (2014).
[14] A. E. Allahverdyan, K. V. Hovhannisyan, A. V. Melkikh, and S. G. Gevorkian, Phys. Rev. Lett. **111**, 050601 (2013).
[15] G. Benenti, K. Saito, and G. Casati, Phys. Rev. Lett. **106**, 230602 (2011).
[16] K. Brandner, K. Saito, and U. Seifert, Phys. Rev. Lett. **110**, 070603 (2013).
[17] K. Brandner and U. Seifert, New. J. Phys. **15**, 105003 (2013).

[18] P. N. Butcher, J. Phys. Condens. Matter **2**, 4869 (1990).
[19] U. Sivan and Y. Imry, Phys. Rev. B **33**, 551 (1986).
[20] T. Christen and M. Büttiker, Europhys. Lett. **35**, 523 (1996).
[21] M. Büttiker, Phys. Rev. B **33**, 3020 (1986).
[22] K. Saito, G. Benenti, G. Casati, and T. Prosen, Phys. Rev. B **84**, 201306(R) (2011).
[23] O. Entin-Wohlman and A. Aharony, Phys. Rev. B **85**, 085401 (2012).
[24] V. Balachandran, G. Benenti, and G. Casati, Phys. Rev. B **87**, 165419 (2013).
[25] M. Büttiker, IBM J. Res. Develop. **32**, 317 (1988).
[26] M. Büttiker, Phys. Rev. Lett. **57**, 1761 (1986).
[27] L. E. Bell, Science **321**, 1457 (2008).
[28] M. Horvat, T. Prosen, G. Benenti, and G. Casati, Phys. Rev. E **86**, 052102 (2012).
[29] J. Stark, K. Brandner, K. Saito, and U. Seifert, Phys. Rev. Lett. **112**, 140601 (2014).